Engineering Structures 121 (2016) 30–41

Contents lists available at ScienceDirect

Engineering Structures

journal homepage: www.elsevier.com/locate/engstruct

Development and validation tests of a dual-core self-centering sandwiched buckling-restrained brace (SC-SBRB) for seismic resistance

Chung-Che Chou [a,b,*], Wen-Jing Tsai [a], Ping-Ting Chung [a]

[a] Department of Civil Engineering, National Taiwan University, Taipei, Taiwan
[b] National Center for Research on Earthquake Engineering (NCREE), Taipei, Taiwan

ARTICLE INFO

Article history:
Received 30 May 2015
Revised 6 April 2016
Accepted 7 April 2016
Available online 7 May 2016

Keywords:
Self-centering sandwiched buckling-restrained brace (SC-SBRB)
High-strength steel tendons
Cyclic test
Residual deformation
Energy dissipation

ABSTRACT

Earthquake-resisting frame systems that are designed based on current seismic provisions provide life safety performance in a large earthquake, but may have significant structural damage or residual drift due to energy dissipation in designated structural members. The damage leads to difficult or expensive repairs after a large earthquake. Therefore, development of a structural system that has both energy dissipation and self-centering properties in earthquakes is needed to improve seismic performances of buildings. This paper presents a viable solution that was validated by multiple cyclic tests of an innovative brace, called a dual-core self-centering sandwiched buckling-restrained brace (SC-SBRB). The proposed brace combines the self-centering property of a dual-core self-centering brace (DC-SCB) and the energy dissipation of a sandwiched buckling-restrained brace (SBRB) together. The dual-core SC-SBRB is essentially a DC-SCB that is positioned concentrically with a SBRB to create both the self-centering and energy dissipation properties in either tension or compression. A 7860 mm-long dual-core SC-SBRB, which uses ASTM A572 Gr. 50 steel as bracing members and ASTM A416 Grade 270 steel tendons as tensioning elements, was cyclically tested six times to validate its kinematics and cyclic performance. The test program demonstrated that the proposed dual-core SC-SBRB provides stable hysteretic responses with appreciable energy dissipation, self-centering behavior and large deformation capacity before low-cycle fatigue failure of the SBRB core.

1. Introduction

Typical earthquake-resisting structural systems, such as the moment-resisting frame (MRF), the concentrically-braced frame (CBF) and the buckling-restrained braced frame (BRBF), generally provide adequate life safety for design level earthquakes [1–3]. The residual drift of these frames that is caused by large energy dissipation or plastic deformation in some structural members during a large earthquake is a critical issue that can make a building difficult and expensive to repair [4,5]. Therefore, development of an earthquake-resisting system that can provide both energy dissipation and self-centering (SC) properties in strong earthquakes is needed to improve its structural damage and post-earthquake performance. This paper presents the development and validation of a novel steel dual-core self-centering sandwiched buckling-restrained brace (SC-SBRB), which combines both the self-centering property of a dual-core self-centering brace (DC-SCB) and the energy dissipation property of a sandwiched buckling-restrained brace (SBRB) together. The proposed dual-core SC-SBRB that is aimed to use conventional steel materials and a post-tensioned (PT) technique can exhibit a flag-shaped hysteretic response without residual deformation in large earthquakes.

A post-tensioned (PT) technique, which applies high-strength steel tendons to compress different structural members together, has been demonstrated to be effective in eliminating residual deformations of structures in cyclic loading [6–11]. However, the slab that is typically constructed in a building frame limits opening of the gap at the beam-to-column interface, significantly affecting the SC property of PT beam-to-column connections under lateral loads [12–14]. A single structural member that is independent of the slab behavior and also provides both the SC and energy dissipation properties to frames is needed. Chou et al. [15–17] proposed a steel dual-core self-centering brace (DC-SCB), which has three sets of conventional steel bracing members, two friction devices and two sets of PT elements. Three sets of steel bracing members and two sets of PT elements that are arranged alongside in the DC-SCB are used to double the axial elongation capacity of the self-

* Corresponding author at: Department of Civil Engineering, National Taiwan University, Taipei, Taiwan. Tel.: +886 2 3366 4349; fax: +886 2 2739 6752.
E-mail address: cechou@ntu.edu.tw (C.-C. Chou).

http://dx.doi.org/10.1016/j.engstruct.2016.04.015
0141-0296/

centering energy-dissipating (SCED) brace [18] when the same PT elements are used in both braces. The mechanics and kinematics of the DC-SCB have been verified successfully from brace member tests by using either fiber-reinforced polymer tendons or high-strength steel tendons as the PT elements. Moreover, multiple tests were conducted on a full-scale one-story, one-bay steel frame with a DC-SCB to validate the system response of the braced frame and study force distributions in framing members as damage progresses in the DC-SCB, beam or columns [19]. Tests confirmed that the DC-SCB in a frame system performs as the mechanics developed, but column base yielding and beam local buckling increase residual drifts of the braced frame. The behavior was observed not only from tests of the DC-SCBF subassembly specimen but also from nonlinear time history analyses of building frames with DC-SCBs [16,19]. Meanwhile, Miller et al. [20] developed a self-centering buckling restrained brace that uses shape-memory alloy bars to provide the SC property and a conventional bucking-restrained brace (BRB) to dissipate seismic energy. The self-centering buckling restrained brace is essentially a BRB acting alongside with shape-memory alloy rods that elongate to create self-centering forces in the SCED brace in either tension or compression. The shape-memory alloy rod not only accommodates large deformation but also dissipates seismic energy due to its flag-shaped hysteretic behavior. By adopting the mechanics of the SCED brace, two works [21,22] also used a BRB for energy dissipation but fiber reinforced polymer composite tendons as tensioning elements. Nonlinear time history analyses of building frames with either self-centering buckling-restrained braces or self-centering braces showed that prototype buildings constructed with these new braces can dissipate significant energy, exhibiting peak drifts similar to conventional systems, and nearly no residual drifts [5,16,23]. This work that investigates a possibility of using a SBRB in a DC-SCB member has never been conducted before, especially for using typical steel tendons as tensioning elements to provide self-centering forces to the brace. In this case, composite tendons or shape-memory alloy rods can be substituted by typical steel tendons to simplify the anchorage of tensioning elements.

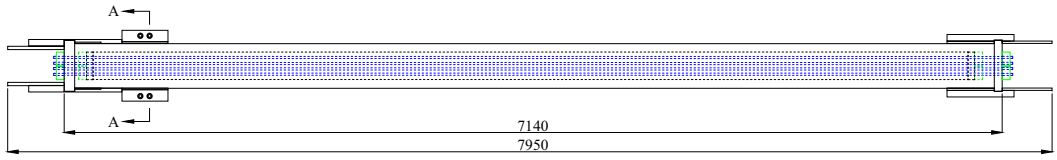

Overall View (unit: mm)

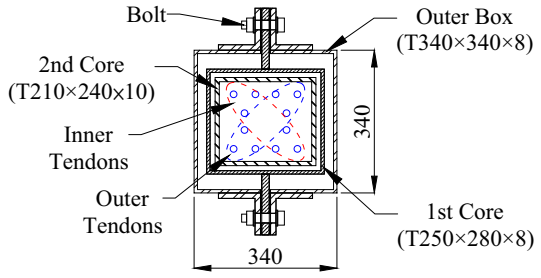

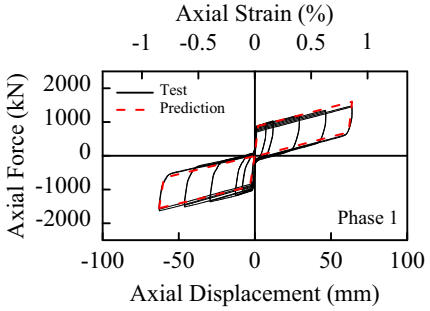

Section A-A (unit: mm)

(a) DC-SCB [17]

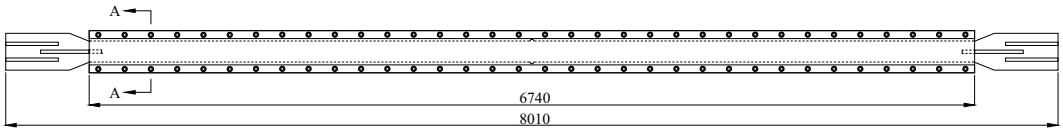

Overall View (unit: mm)

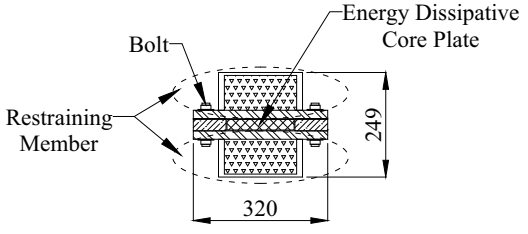

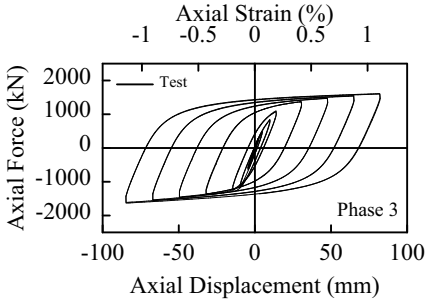

(b) SBRB [24]

Fig. 1. Configurations and responses of a DC-SCB and a SBRB.

The objective of this work is to develop an earthquake-resistant SC-SBRB that uses the kinematics of the DC-SCB [17] to provide SC behavior and the plate yielding mechanism of the SBRB [24] to provide energy dissipation. Since the SC behavior can be achieved by utilizing two sets of tensioning elements and three sets of box members in the DC-SCB (Fig. 1(a)), typical ASTM A416 Grade 270 steel tendons instead of shape-memory alloy rods or composite tendons can be used in the proposed dual-core SC-SBRB. Moreover, a friction device that provides energy dissipation in the original DC-SCB is substituted by the SBRB in the dual-core SC-SBRB to minimize reduction of energy dissipation due to gradual abrasion of asperities of brass shim plates in multiple tests. Compared to conventional BRBs that have a steel core inserted into a concrete-filled steel member, using bolts to sandwich a core plate by a pair of restraining members in the SBRB (Fig. 1(b)) enables fast assembly and produces stable hysteretic yielding behavior [24–26]. The additional advantage is the ability to disassemble the SBRB in the field after a large earthquake, which enables replacement of only the core plate independently of restraining members for reuse. In this study, a 7860 mm-long dual-core SC-SBRB was designed, fabricated and tested in multiple times to validate its force-transfer mechanism, cyclic performance and durability. The proposed dual-core SC-SBRB can be used in place of a conventional steel brace, BRB or SCB without modification to the rest of the braced frame configuration.

2. Kinematics of a dual-core self-centering sandwiched buckling-restrained brace (SC-SBRB)

The configuration of a dual-core SC-SBRB (Fig. 2) has a SBRB inside a DC-SCB that creates self-centering forces in either tension or compression. The DC-SCB positions the first core, second core, outer box and two sets of tensioning elements in parallel to form its force transfer mechanism [15–17,19]. The SBRB uses two identical restraining members to sandwich an energy dissipative core plate [24–26]. The proposed SC-SBRB positions a SBRB concentrically with a DC-SCB so that the first core, second core, outer box and tensioning elements in the proposed brace function as those in the DC-SCB. Energy dissipation of the proposed brace is provided by a core plate of the SBRB. Two inner end plates are placed on each end of the second core, and two outer end plates are placed on each end of the outer box and the first core (Fig. 2(a)). The outer tendons are anchored to the left inner end plate and the right outer end plate; the inner tendons are anchored to the left outer end plate and the right inner end plate. Both ends of tendons are anchored to ends of different bracing members to double the elongation capacity of the self-centering brace under loading [15–17,19]. These tendons are post-tensioned to compress bracing members against end plates and are elongated to provide the SC property when the brace deforms axially. A SBRB that is positioned inside a DC-SCB (Fig. 2) is composed of an energy dissipative core plate and a pair of buckling-restraining members sandwiched together by high-strength bolts [24]. Oblique lines that surround an energy dissipative core plate in Figs. 3 and 4 represent a set of restraining members (Fig. 2(b)) that are connected by high-strength bolts. Both ends of the SBRB core are connected to the first core and the outer box of the DC-SCB, respectively, so that some external loads can be directed to the SBRB when the dual-core SC-SBRB is in loading. Numerous works have demonstrated satisfactory seismic performances of SBRBs or frames with SBRBs under multiple tests [24–26]; no gradual energy reduction as seen in DC-SCB tests is observed in SBRB tests. Therefore, it is expected that using a SBRB as energy dissipation in a DC-SCB can eliminate the behavior of energy reduction as seen in the frictional device [17].

The basic concept of the dual-core SC-SBRB, including a relative movement between the first core and the outer box, is similar to that of the original DC-SCB. Fig. 4 shows the kinematics of a dual-core SC-SBRB in tensioning and compression. Fig. 4(a) shows unstrained situation of the proposed brace. The left end of an energy dissipative core plate of the SBRB that is welded to the first core of the DC-SCB moves freely with respect to the outer box and the left outer end plate of the DC-SCB. The right end of an energy dissipative core plate of the SBRB that is welded to the outer box of the DC-SCB moves freely with respect to the first core and the right outer end plate of the DC-SCB. The outer tendons are anchored to the left inner end plate and the right outer end plate; the inner tendons are anchored to the left outer end plate and the right inner end plate. When the initial PT force and the force

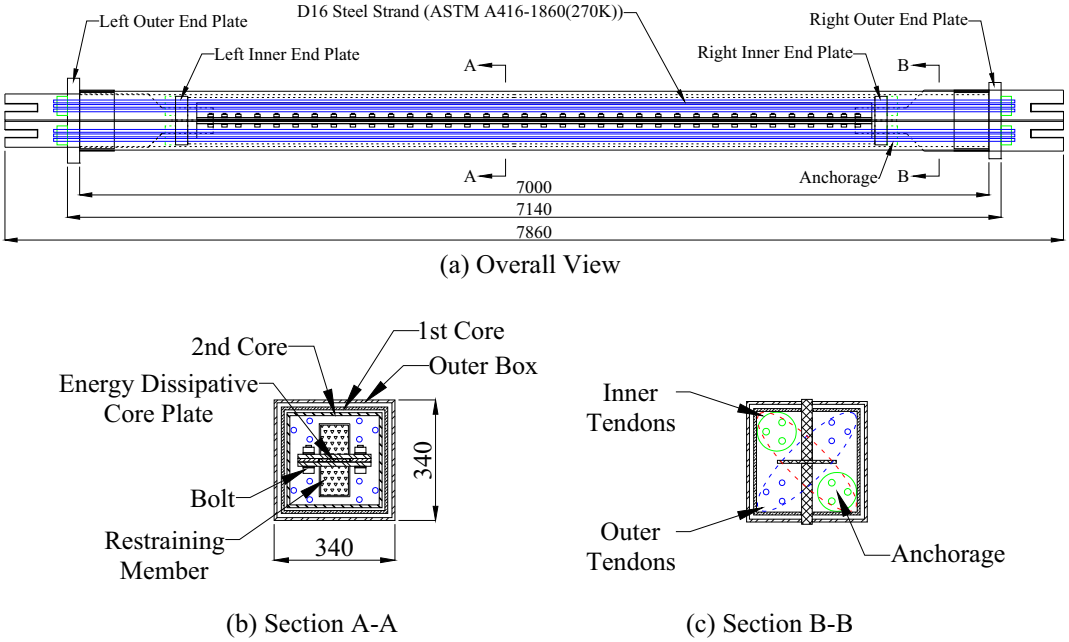

Fig. 2. A proposed dual-core SC-SBRB (unit: mm).

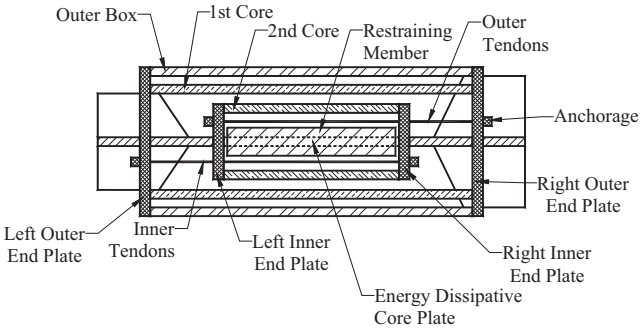

Fig. 3. A schematic of the dual-core SC-SBRB.

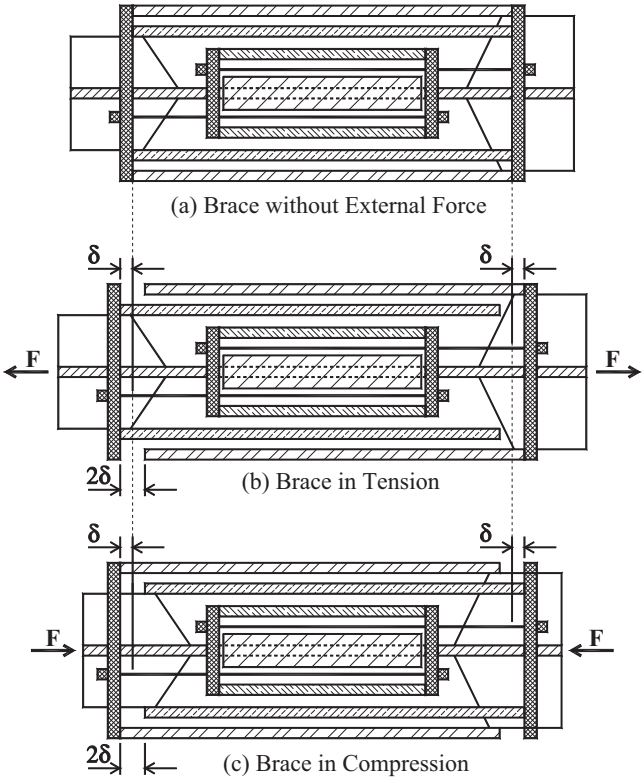

Fig. 4. Kinematics of the dual-core SC-SBRB.

required to activate the SBRB are exceeded by a tensile load F, the outer box and the first core begin to move with respect to the second core. The relative displacement δ between the outer box and the second core and the equal displacement between the first core and the second core result in an axial displacement of 2δ in the brace (Fig. 4(b)), which doubles the elongation δ of the outer and inner sets of tendons. The axial displacement of 2δ of the dual-core SC-SBRB equals the elongation of the SBRB core for energy dissipation. The outer end plates move with respect to the bracing members such that tensile forces in steel tendons increase with δ, providing elastic restoring forces to the dual-core SC-SBRB in tension. Complete re-centering occurs as long as the tendons remain elastic and the initial PT force exceeds the force that is required to activate the SBRB.

When a load F applied in the opposite direction exceeds the sum of the initial PT force and the force needed to activate the SBRB, the outer end plates begin to move with respect to the outer box and the first core (Fig. 4(c)). The elongation δ in each set of tendons causes an axial deformation of 2δ in the SBRB, which leads to axial shortening of the SBRB core; buckling of the core plate is effectively prevented by a pair of restraining members. The dual-core SC-SBRB returns to its original position when a load is removed.

3. Hysteretic response of the dual-core SC-SBRB

3.1. A dual-core SC-SBRB under initial PT forces

The dual-core SC-SBRB is under an initial PT force to maintain all bracing members and end plates together. The initial PT force applies compressive forces $P_{1c,in}$, $P_{2c,in}$, $P_{ob,in}$ and $P_{BRB,in}$ to three bracing members of the DC-SCB and a core plate of the SBRB based on the respective axial stiffness of each member:

$$P_{1c,in} = \frac{\frac{n}{2}T_{in} \times K_{1c}}{K_{1c} + K_{ob} + K_{yt,B}}; \quad P_{2c,in} = \frac{n}{2}T_{in}; \quad P_{ob,in} = \frac{\frac{n}{2}T_{in} \times K_{ob}}{K_{1c} + K_{ob} + K_{yt,B}};$$
$$P_{BRB,in} = \frac{\frac{n}{2}T_{in} \times K_{yt,B}}{K_{1c} + K_{ob} + K_{yt,B}} \tag{1}$$

where K_{1c}, K_{ob} and $K_{yt,B}$ are the axial stiffness of the first core, the outer box and the core plate, respectively; T_{in} is the initial PT force in each tendon and n is a total number of tendons. A initial shortening of the member caused by the initial PT force is

$$\delta_{1c,in} = \delta_{ob,in} = \delta_{BRB,in} = \frac{\frac{n}{2}T_{in}}{K_{1c} + K_{ob} + K_{yt,B}}; \quad \delta_{2c,in} = \frac{\frac{n}{2}T_{in}}{K_{2c}} \tag{2}$$

where $\delta_{1c,in}$, $\delta_{2c,in}$, $\delta_{ob,in}$ and $\delta_{BRB,in}$ are the initial shortening of the first core, the second core, the outer box and the SBRB core, respectively, and K_{2c} is the axial stiffness of the second core.

3.2. A dual-core SC-SBRB under earthquake loads

The hysteretic response of the dual-core SC-SBRB (Fig. 5(a)) is attributed to a bi-linear elastic behavior of the DC-SCB (Fig. 5(b)) and a hysteretic plastic behavior of the SBRB (Fig. 5(c)). The hysteretic response of the DC-SCB that has no energy dissipation is illustrated in Fig. 5(b), in which a tensile activation force of the DC-SCB when the first core and the outer box start moving is

$$P_{dt,S} = \frac{nT_{in}}{2} \tag{3}$$

The tensile axial deformation, δ_{dt}, corresponding to the tensile activation force is the same as the initial shortening, $\delta_{ob,in}$, so that the elastic axial stiffness of the brace in tension is expressed as $K_{it,S}$ ($=P_{dt,S}/\delta_{dt}$). When the brace load exceeds the tensile activation force, a post-elastic axial stiffness of the brace, $K_{pt,S}$, which is associated with force transfer from one end to the other end of the brace through inner tendons, outer tendons and second core (Fig. 4(b)), is calculated as

$$K_{pt,S} = \frac{1}{\frac{1}{\frac{n}{2}K_{ten}} + \frac{1}{K_{2c}} + \frac{1}{\frac{n}{2}K_{ten}}} \tag{4}$$

where K_{ten} is the axial stiffness of one tendon. The behavior of the DC-SCB in compression is similar to that in tension (Fig. 5(b)) except that all box members carry compression forces as shown in Fig. 4(c). The activation force of the DC-SCB in compression, $P_{dc,S}$, approximates that in tension (Eq. (3)), and the corresponding axial deformation, δ_{dc}, is

$$\delta_{dc} = \frac{P_{dc,S} - P_{1c,in}}{K_{1c}} + \frac{P_{dc,S} - P_{ob,in}}{K_{ob}} \tag{5}$$

The elastic axial stiffness of the DC-SCB in compression is $K_{ic,S}$ ($=P_{dc,S}/\delta_{dc}$). When the compressive activation force is reached, a post-elastic axial stiffness of the DC-SCB is

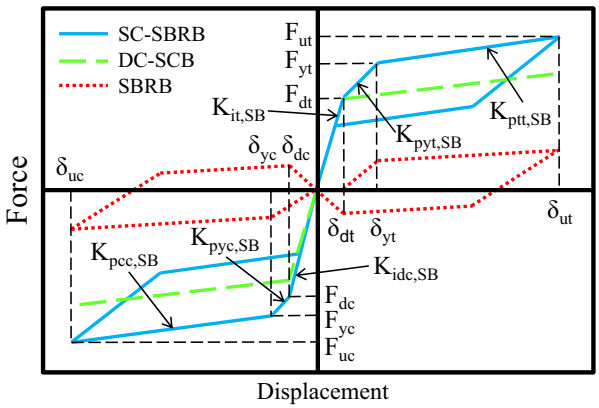

(a) Dual-Core SC-SBRB

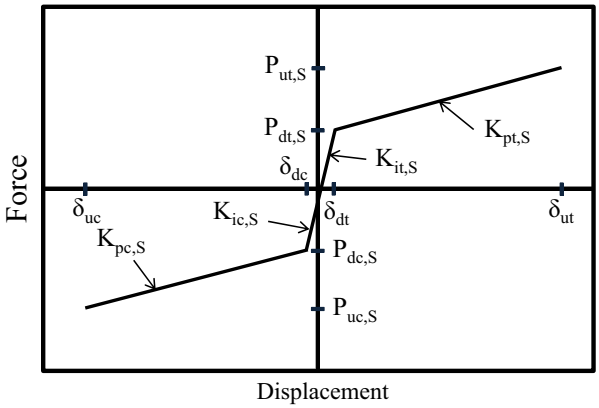

(b) DC-SCB without Energy Dissipation

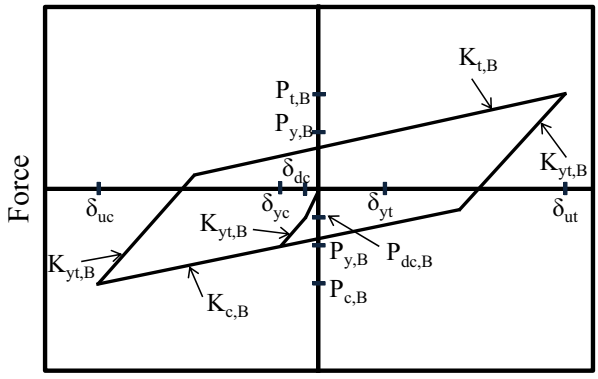

(c) SBRB

Fig. 5. Hysteretic response of the dual-core SC-SBRB.

$$K_{pc,S} = \frac{1}{\frac{1}{K_{1c}} + \frac{1}{\frac{n}{2}K_{ten}} + \frac{1}{K_{2c}} + \frac{1}{\frac{n}{2}K_{ten}} + \frac{1}{K_{ob}}} \tag{6}$$

The SBRB remains elastic right after the dual-core SC-SBRB is activated so that a tri-linear instead of bi-linear force–deformation relationship as observed in the DC-SCB is obtained (Fig. 5(a)). The core of the SBRB is in compression after the initial PT force, $P_{BRB,in}$, so the activation force of the dual-core SC-SBRB in compression is

$$\begin{aligned} F_{dc} &= P_{dc,S} + P_{dc,B} \\ &= \left(\frac{n}{2}T_{in}\right) + (P_{BRB,in} + K_{yt,B} \times \delta_{dc}) \end{aligned} \tag{7}$$

where $P_{dc,S}$ is the activation force of the DC-SCB and $P_{dc,B}$ is the axial force of the SBRB at the activation. The activation force in tension is less than that in compression because the SBRB returns back to its original position (i.e. zero force) when the tensile activation force, F_{dt}, is reached

$$F_{dt} = P_{dt,S} = \frac{n}{2}T_{in} \tag{8}$$

The hysteretic response of the SBRB is illustrated in Fig. 5(c), which is similar to that of a conventional BRB. The core of the SBRB is initially shortened by a value of $\delta_{BRB,in}$ due to the initial PT force applied to the SBRB, $P_{BRB,in}$, so that the tension and compression yield displacements of the dual-core SC-SBRB differ by $2\delta_{BRB,in}$ and are expressed as

$$\delta_{yt} = \delta_y + \delta_{BRB,in} \tag{9}$$

$$\delta_{yc} = \delta_y - \delta_{BRB,in} \tag{10}$$

where δ_{yt} and δ_{yc} are the yield displacements of the dual-core SC-SBRB in tension and compression, respectively, and δ_y is the yield displacement of the SBRB. The dual-core SC-SBRB starts to dissipate energy when the core of the SBRB is loaded beyond its yield displacement, δ_y. The post-elastic stiffness of the dual-core SC-SBRB (Fig. 5(a)) is the summation of that of the DC-SCB (Fig. 5(b)) and the SBRB (Fig. 5(c)) in the corresponding loading stage.

4. Test program

The test program consisted of cyclic tests of a 7.86 m-long dual-core SC-SBRB specimen, which had a SBRB inside a DC-SCB (Fig. 2). The DC-SCB had a first core of T300 × 300 × 8 mm, a second core of T268 × 268 × 8 mm and an outer box of T340 × 340 × 8 mm (Table 1(a)). The first core and outer box were 7000 mm long and the second core was 5720 mm long. The brace had 12 seven-wire ASTM A416 Grade 270 steel tendons (Table 1(b)), and only six tendons were anchored outside the outer end plates (Figs. 2 and 3). The SBRB had a core plate of 8 × 86 mm and two identical restraining members connected by 72 S10T bolts with a diameter of 16 mm. Each restraining member was composed of a 12 mm-thick flat plate welded with a channel of 86 × 86 × 4 mm (Table 1(a)). The mortar with a measured compressive strength of 60 MPa was filled into the channel. The dual-core SC-SBRB specimen was fabricated by a local steel fabricator and post-tensioned at the National Center for Research on Earthquake Engineering (NCREE), Taiwan. The specimen was placed in the test setup (Fig. 6), which included one steel box column pin-supported to the laboratory floor and attached to four 1000-kN hydraulic actuators. Positive drift means that actuators push the column to the right so that the brace is in compression. The specimen was positioned at an incline of $\theta = 26°$ with both ends welded to dual gusset plates [25], which were designed to remain elastic at ultimate strength level. The relationship between brace strain ε_c and column drift angle β was determined based on axial deformation in the specimen [17]:

$$\varepsilon_c = \frac{L_b\beta}{2L_y}\sin 2\theta \tag{11}$$

where L_b (=8965 mm) is the length between working points chosen at the intersection of the centerlines of the column, SC-SBRB and base (Fig. 6(b)), and L_y (=6484 mm) is the tendon length. The tendon strain is the summation of strains caused by the initial PT force and $0.5\varepsilon_c$ during the test.

To achieve the self-centering behavior of the specimen, the initial PT force of six steel tendons was set to 415 kN that exceeded an expected axial force of 400 kN of the SBRB at a lateral drift of 2%. Therefore, the SBRB core was 8 × 86 mm that could create a yield

Table 1
Sizes and material properties of a dual-core SC-SBRB specimen.

Dual-core SC-SBRB	Material	Member	Size (mm)	Length (mm)	Yield strength (MPa)	Ultimate strength (MPa)	Elastic modulus (GPa)
(a) Steel bracing members and materials							
DC-SCB	A572 Gr. 50	1st core	T300 × 300 × 8	7000	369	487	206
		2nd core	T268 × 268 × 8	5720	369	487	206
		Outer box	T340 × 340 × 8	7000	369	487	206
SBRB	A572 Gr. 50	Core plate	8 × 86	7860	370	510	212
	A572 Gr. 50	Face plate	12 × 206	5650	409	517	206
	A36	Channel	86 × 86 × 4	5650	235	399	197

Tendons	Material	Elastic modulus (GPa)	Diameter (mm)	Area (mm^2)	Number	Length (mm)	Yield strength (MPa)	Ultimate strength (MPa)
(b) Steel tendons								
Outer tendons	A416 Gr. 270	198	15.2	144	6	6516		
Inner tendons					6	6484	1358	1865

force of 256 kN. The design force of the specimen at a target lateral drift of 2% was about 1564 kN (Table 2(a)) in accordance with a tendon strain value of 0.78%, which was much lower than 1.26% if only a single-core member was used in the SCB.

4.1. Six loading phases

The dual-core SC-SBRB specimen was subjected to six phase tests. In Phase 1 test, the loading protocol that was based on AISC seismic provisions [27] consisted of two cycles per column drift of 0.09%, 0.18%, 0.36%, 0.5%, 1%, 1.5% and 2%. The actuator displacement rate was 0.393 mm/s for column drifts less than 1% and 0.786 mm/s for other column drifts. The specimen was then subjected to a 15 low-cycle fatigue test at a column drift of 1.5% (Phase 2). The objective of the test was to evaluate the durability of the dual-core SC-SBRB and the tendon-anchorage system. The specimen was reloaded in Phase 3 and 4 tests using the Phase 1 loading protocol from a column drift of 0.09 up to 2.5% to investigate the effects of steel tendon yielding on the brace behavior. The specimen was then subjected to a 30 low-cycle fatigue test at a column drift of 1.5% (Phase 5). After the Phase 5 test, an additional low-cycle fatigue test at a column drift of 2.5% was conducted on the specimen until failure occurred (Phase 6). All these six phase tests could examine the mechanics, durability and cyclic behavior of the dual-core SC-SBRB.

4.2. Phase 1 test results

Fig. 7 shows the actuator force *versus* displacement responses of the dual-core SC-SBRB specimen in six phase tests; Fig. 8 shows the corresponding axial force *versus* axial displacement responses of the specimen. The axial deformation is measured from displacement transducers (marked as L series) positioned on both ends of the dual-core SC-SBRB (Fig. 6(b)). Fig. 9(a) and (b) are schematic diagrams of the brace under tension and compression, respectively. Displacement transducers, L1, L2, L3 and L4 measure relative displacement between the outer end plate and the outer box. When the brace is in tension (Fig. 9(a)), the left outer end plate separates from the outer box (Fig. 10(a)) and no displacements in L1 or L2 occur (Fig. 10(b)). The displacement in L3 or L4 is the axial deformation of the brace in tension (Fig. 9(c)). As the brace is compressed (Fig. 9(b)), the outer box bears against the left outer end plate and no displacements in L3 or L4 occur (Fig. 10(c)). The right outer end plate separates from the outer box (Fig. 10(d)), and the displacement in L1 or L2 is the axial deformation of the brace in compression (Fig. 9(c)). The gap opening at both ends of the dual-core SC-SBRB is similar (Fig. 9(d)), indicating a similar force increment in PT elements in either tension or compression. The behavior is consistent with the kinematics of the brace as shown in Fig. 4.

The brace behavior in Phase 1 test was close to the prediction except for energy dissipation (Fig. 8(a) and Table 2) because the isotropic strain hardening of steel was not considered in the model. At 2% lateral drift, the maximum tendon strain obtained from strain gages was close to the yield strain of 0.7% (Fig. 11(a)), indicating no yielding in tendons. The pre-tension force, however, decreased slightly as drift increased in Phase 1 test (Fig. 11(b)) owing to slippage of the tendon-anchorage system, which occurred whenever the axial load in tendons exceeded the peak load in the previous drift cycles. The reduction was about 14%, but the pre-tension force after loss (358 kN) was still larger than the axial force of the SBRB (298 kN), indicating a good self-centering behavior as seen in the hysteretic response (Fig. 8(a)). The residual axial deformation of the specimen was less than 2 mm after the Phase 1 test (Fig. 11(c)).

Contribution of the SBRB (Fig. 11(d)) was obtained by subtracting the bilinear elastic response of the DC-SCB from the overall hysteretic response of the dual-core SC-SBRB. The force in the SBRB increased with the increase of axial deformation. Whenever the dual-core SC-SBRB unloaded to the axial activation displacement of δ_{dt} or δ_{dc}, the gap at both ends of the brace closed, decreasing forces carried by the SBRB but adding forces to other bracing members. Table 2(b) lists the axial force and axial stiffness of the dual-core SC-SBRB, which was calculated based on the 2% cyclic test. The activation force, elastic and post-elastic axial stiffnesses of the brace obtained from the test are similar to those calculated according to the mechanics of the dual-core SC-SBRB in different loading stages (Fig. 5). Note that the elastic axial stiffness of the brace is different in tension and compression due to the corresponding activation deformation calculated based on Eqs. (2) and (5), respectively.

4.3. Phase 2–6 test results

Fig. 7(b) to (f) shows the actuator force *versus* displacement responses of the specimen from two to six phase tests, and Fig. 8 (b) to (f) shows the corresponding axial force *versus* axial displacement responses of the specimen. The dual-core SC-SBRB specimen exhibited repeatable hysteretic responses in a 15 low-cycle fatigue test (Fig. 8(b)); no stiffness or force degradation was observed in the test. Therefore, the specimen was reloaded with the AISC loading protocol up to a lateral drift of 2.5% in Phase 3 and 4 tests. When the specimen was overloaded to 2.5% drift cycles, the tendon strain was 0.81%, slightly larger than its 0.7% yield capacity. Fig. 12 (a) shows variation of the initial PT force after each phase test; minor loss of the initial PT force was observed when the tendon was slightly loaded beyond its yield capacity in Phase 3 and 4 tests.

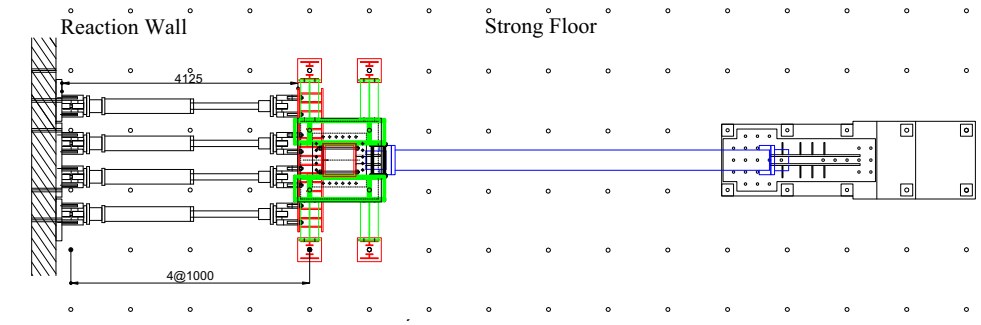

(a) Top View

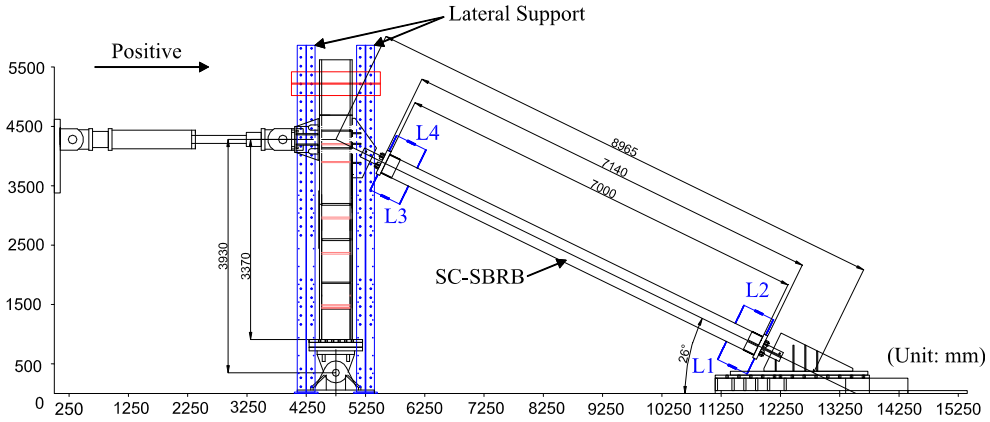

(b) Side View

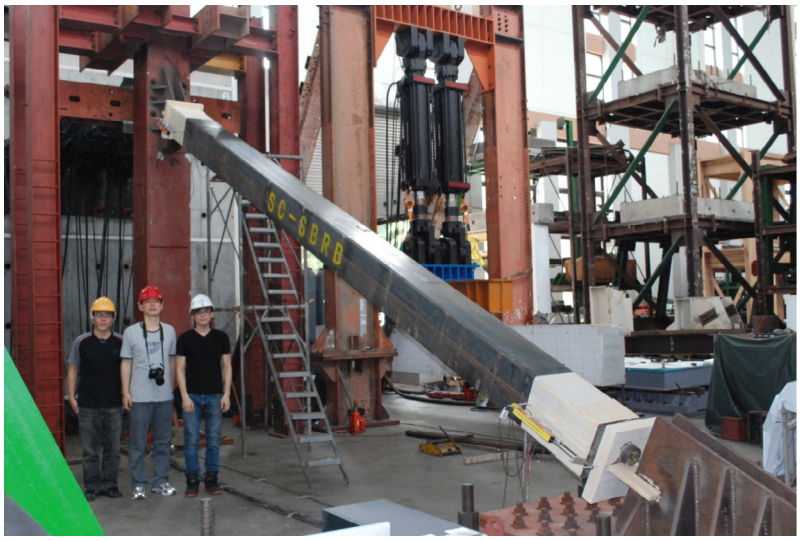

(c) 2% Drift

Fig. 6. Test setup and response.

Although the initial PT force decreased slightly due to tendon yielding, the self-centering and energy-dissipation properties of the specimen were maintained throughout the tests (Fig. 8 (c) and (d)). The maximum axial force of the brace at 2.5% drift was 1650 kN without damage in tensioning elements, anchorages or a core plate. Then, the specimen was subjected to a 30 low-cycle fatigue test at 1.5% drift to examine its post-earthquake performance (Phase 5). The specimen exhibited similar hysteretic responses in Phase 5 and Phase 2 tests (Fig. 8(b) and (e)), indicating a reliable brace even after multiple tests. The specimen showed no damage after completing a 30 low-cycle fatigue test (Phase 5) so that a low-cycle fatigue test at 2.5% drift was conducted on the same specimen until failure occurred (Phase 6). The specimen first experienced one complete loading cycle without damage and then exhibited a sudden fracture of the SBRB core in the second cycle. A sudden drop in tension force decreased energy dissipation as seen in Fig. 8(f); the peak compression force was maintained because a fracture of a SBRB core that was confined within restraining members was closed to carry axial forces. A significant reduction in the activation force, peak tension force and energy dissipation was clearly observed in the third cycle of Phase 6 test. Minor energy dissipation that was observed in the rest of test cycles was proba-

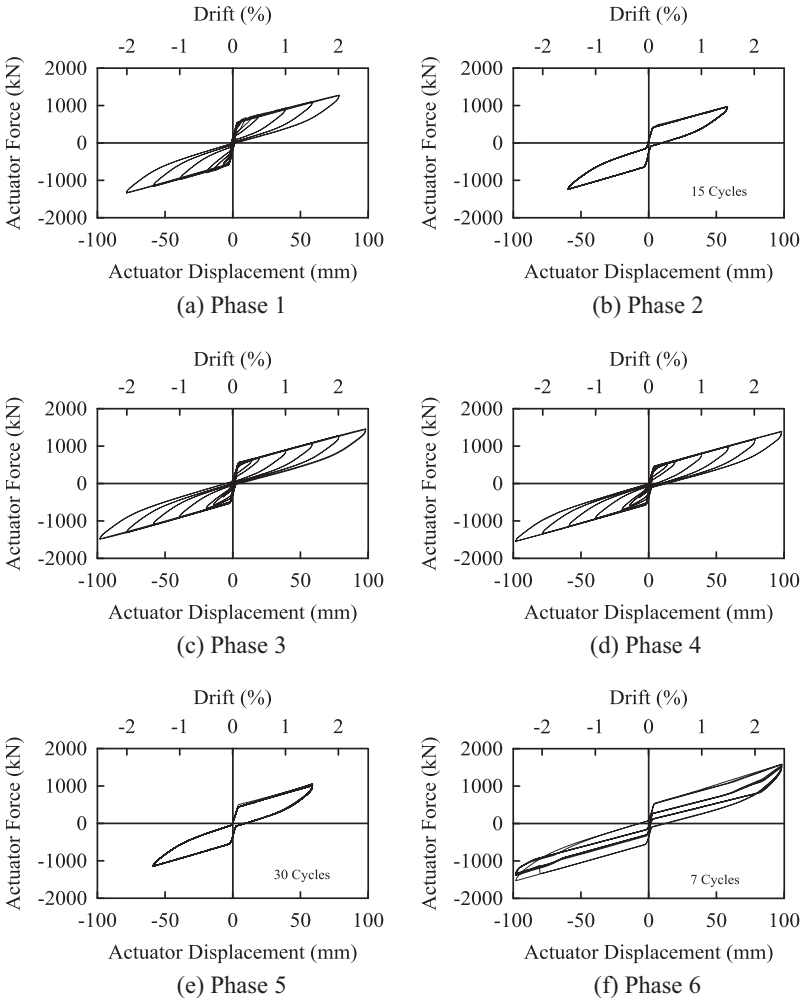

Fig. 7. Actuator force *versus* displacement relationships of the dual-core SC-SBRB (Phase 1–6 test results).

bly caused by friction in steel bracing members. No damage in tensioning elements, tendon-anchorage systems or bracing members was found after completing six phase tests.

The original DC-SCB uses a friction device for energy dissipation, but friction force decreases gradually due to gradual abrasion of brass shim plates in the friction device. Reduction in friction forces also decreases energy dissipation. The proposed dual-core SC-SBRB, however, uses plate yielding instead of friction for energy dissipation, excluding gradual reduction of energy dissipation before failure. Fig. 12(b) shows energy dissipation computed for the first 1.5% drift cycle in each test phase; the corresponding equivalent viscous damping ratio is computed based on [28]:

$$\xi_{eq} = \frac{A_h}{2\pi F_m \Delta_m} = \frac{A_h}{4\pi A_e} \tag{12}$$

where F_m is the average of positive and negative peak brace forces, Δ_m is the average of positive and negative peak brace displacements, A_h is the energy dissipation in one cycle, and A_e is the elastic strain energy. The dual-core SC-SBRB specimen provides stable energy dissipation in each test phase, without any sign of energy degradation. The total energy that the dual-core SC-SBRB dissipates in all six phase tests is 3651 kN-m, which is about 12.2 times that in Phase 1 test. The equivalent viscous damping ratio is 12–13% in the first three test phases and increases slightly in subsequent test phases due to strain hardening of a steel core.

5. Summary of a dual-core SC-SBRB design procedure

The proposed dual-core SC-SBRB is composed of a DC-SCB and a SBRB, which are assembled together by using high-strength steel tendons as tensioning elements. Multiple tests show that the dual-core SC-SBRB has stable and reliable flag-shaped hysteretic responses with good self-centering and energy-dissipation properties. Based on this study, a step-by-step design procedure for the proposed brace is summarized as follows:

(1) Determine ultimate axial force F_u and strain ε_u of the brace at a target design drift.
(2) Two steel inner cores and one outer box are designed to sustain the axial force of F_u based on the AISC-LRFD manual [29].
(3) Determine a tendon force increment, ΔF, from the initial PT force stage to the target drift level based on

$$\Delta F = 0.5\varepsilon_c L_y K_{pt} \tag{13}$$

where *Kpt* is the post-elastic stiffness of the DC-SCB in either tension or compression.
(4) The activation force is obtained by subtracting force increments of tendons (Eq. (13)) and a SBRB core from the target axial force F_u.
(5) Determine an initial PT force of one tendon, T_{in}, and the number of tendons, n, from Eq. (3).

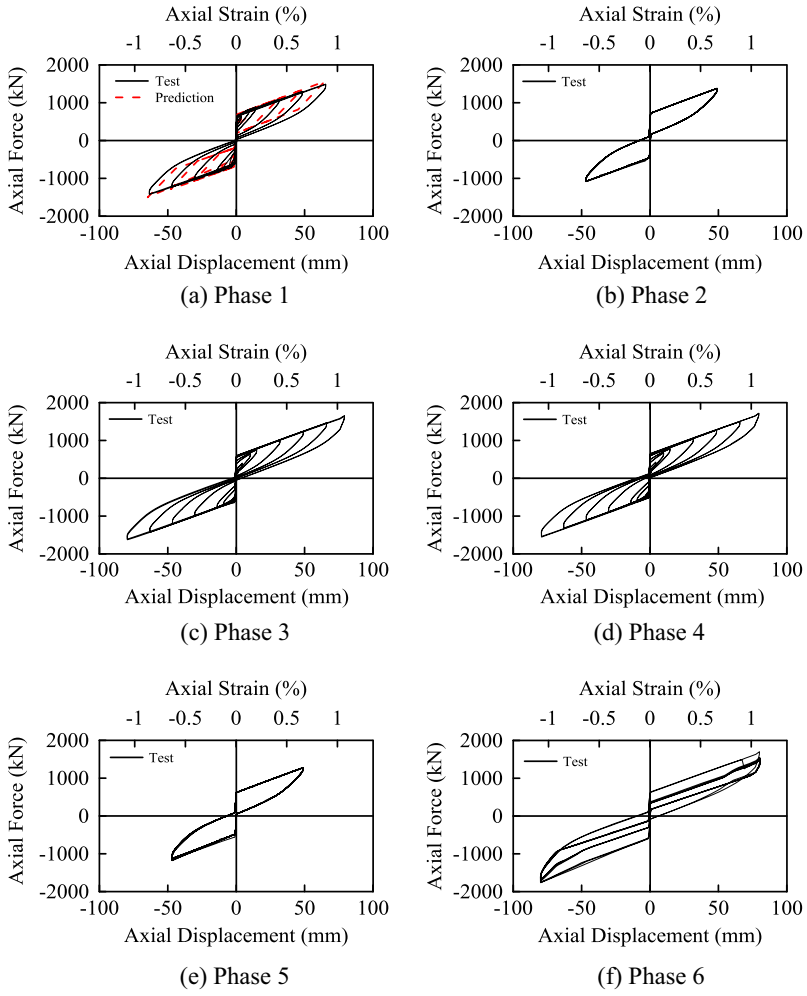

Fig. 8. Axial force *versus* axial displacement relationships of the dual-core SC-SBRB (Phase 1–6 test results).

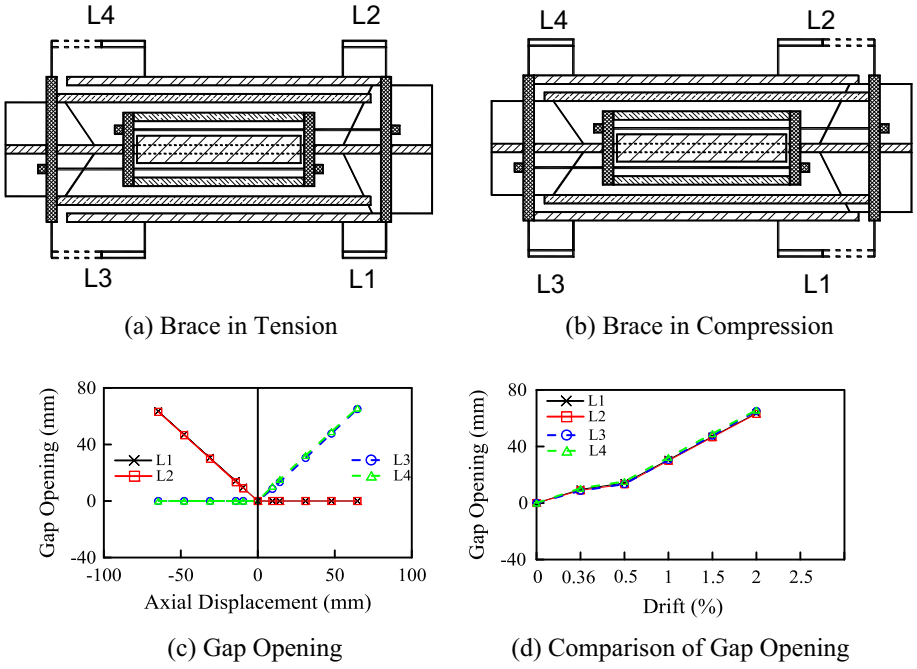

Fig. 9. Schematic and responses of gap opening of the dual-core SC-SBRB (Phase 1 test).

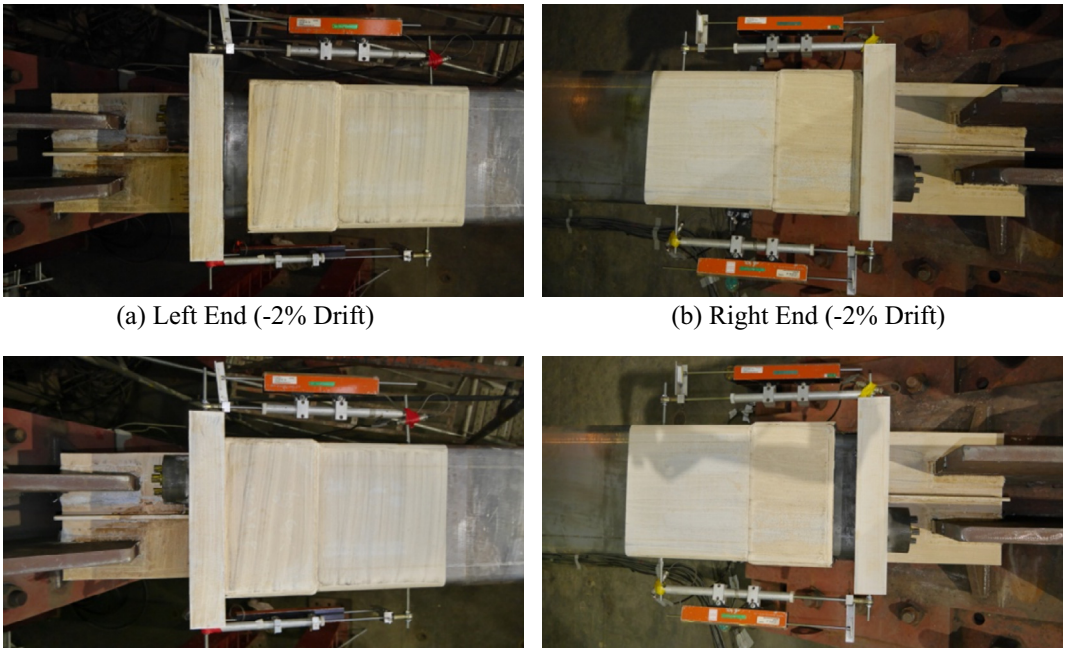

(a) Left End (-2% Drift) (b) Right End (-2% Drift)

(c) Left End (+2% Drift) (d) Right End (+2% Drift)

Fig. 10. Observed gap opening at both ends of the dual-core SC-SBRB (Phase 1 test).

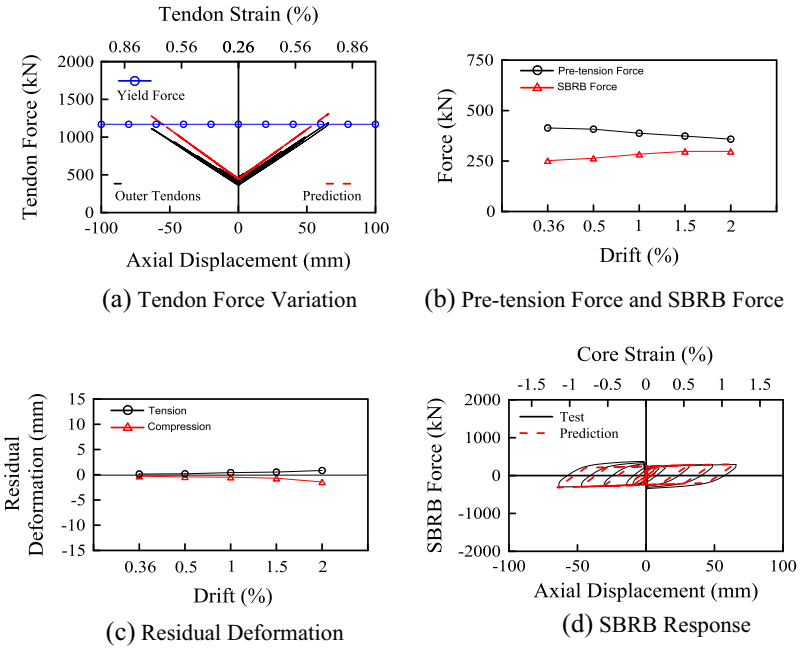

(a) Tendon Force Variation (b) Pre-tension Force and SBRB Force

(c) Residual Deformation (d) SBRB Response

Fig. 11. Responses of the SC-SBRB (Phase 1 test).

(6) Calculate tendon strain at the target drift by the summation of strains caused by the initial PT force and $0.5\varepsilon_c$. If the calculated strain exceeds the design limit of tendon strain capacity, it is suggested to increase the number of tendons or length of the brace.

(7) Determine a cross sectional area of a SBRB core such that its ultimate force at the target drift is lower than the initial PT force ($=nT_{in}/2$) to assure self-centering responses. Determine the size of restraining members based on $P_e/P_y > 2.5$ [24], where P_e is the Euler buckling load of restraining members and P_y is the yield force of a core plate.

(8) Calculate the activation deformation, activation force and post-elastic stiffness of the brace based on Eqs. (4) to (10).

(9) Once design parameters are determined from steps 1 to 8, a specific flag-shaped hysteretic response of the dual-core SC-SBRB can be obtained as shown in Fig. 5.

Note that the design procedure in this section is proposed only for selection of a dual-core SC-SBRB. Although the hysteretic behavior of the SC-SBRB is similar to other types of self-centering braces, nonlinear dynamic analyses of buildings equipped with such braces under a set of representative ground motions may

Table 2
Prediction and test of a dual-core SC-SBRB (Phase 1 test).

Drift (%)		0.36	0.5	1	1.5	2
(a) Peak force at each drift						
Axial tension force	Prediction (kN)	815	880	1107	1335	1564
	Test (kN)	825	886	1092	1297	1486
	Prediction/Test	0.99	0.99	1.01	1.03	1.05
Axial compression force	Prediction (kN)	797	858	1072	1287	1502
	Test (kN)	792	840	1036	1231	1415
	Prediction/Test	1.01	1.02	1.03	1.05	1.06

Dual-core SC-SBRB	F_{dt} (kN)	$K_{it,SB}$ (kN/mm)	$K_{ptt,SB}$ (kN/mm)	F_{dc} (kN)	$K_{idc,SB}$ (kN/mm)	$K_{pcc,SB}$ (kN/mm)
(b) Activation force and axial stiffness (2% drift)						
Prediction	626	596	14	604	309	13
Test	644	585	13	613	370	14
Prediction/Test	0.97	1.02	1.08	0.99	0.84	0.93

Drift (%)		0.5	1	1.5	2
(c) Energy dissipation at each drift					
Energy dissipation	Prediction (kN-m)	2.5	16	31	51
	Test (kN-m)	7.5	25	44	66
	Prediction/Test	0.33	0.65	0.7	0.77
Equivalent viscous damping ratio	Prediction (%)	3.4	8	8.2	8.6
	Test (%)	9.7	12	12	11
	Prediction/Test	0.35	0.67	0.68	0.78

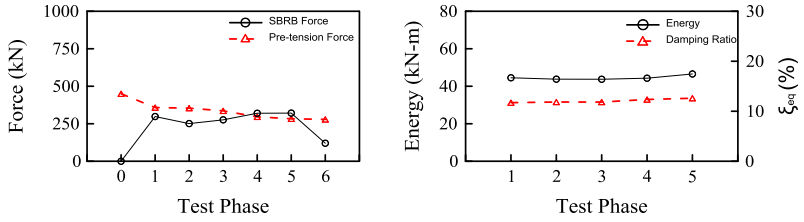

(a) Pre-tension Force and SBRB Force (b) Energy Dissipation

Fig. 12. Responses of the SC-SBRB in each test phase.

provide design verification [5,16,19,23]. An energy-based method that could be applied to steel frame design or analysis may be considered in selection of parameters of braces along the building height [30,31]. Within the paper content, the reader is directed to an on-line thesis [32], where the specimen, fabrication, tests and specimen responses are fully described.

6. Conclusions

A dual-core self-centering sandwiched buckling-restrained brace (SC-SBRB) that combines both the self-centering behavior of the DC-SCB and the energy dissipation of the SBRB together is developed and validated in this study. The DC-SCB has three sets of steel bracing members and two sets of tensioning elements that are arranged in parallel to increase its elongation capacity for self-centering response. The SBRB that has a single core plate sandwiched by a pair of restraining members is positioned inside a DC-SCB to dissipate seismic energy. A 7860 mm long full-scale SC-SBRB was designed, fabricated and tested to evaluate its mechanics, cyclic behavior and durability.

Multiple tests confirm that the dual-core SC-SBRB performs as predicted by the mechanics and its elongation capacity is doubled by serial deformations of two tensioning element sets. Therefore, the ASTM A416 Grade 270 high-strength steel tendons instead of superelastic nickel-titanium shape memory alloy rods or composite tendons can be used to provide re-storing forces to the new brace in seismic loadings. A good self-centering property of the new brace was ensured within the target lateral drift of 2.5% without failure. The residual deformation after load removal in each test phase was very small, less than 3% of the maximum axial deformation. A fracture of a SBRB core occurred after the brace experienced three increasing cyclic loading tests and 46 low-cycle fatigue tests, indicating abundant and stable energy dissipation in earthquakes. Therefore, the novel dual-core SC-SBRB is a very attractive steel brace compared to BRBs [2–4,24,33–35] or SCBs [15–23] because it has good self-centering and energy-dissipation properties in multiple tests.

Acknowledgments

The authors would like to thank the National Science Council Taiwan for financially supporting this research under Contract No. NSC 102-2625-M-002-002.

References

[1] Roeder CW, Lehman DE, Yoo JH. Improved seismic design of steel frame connections. Steel Struct 2005;5:141–53.
[2] Kasai K, Ooki Y, Ito H, Motoyui S, Hikino T, Sato E. Full-scale tests of passively-controlled 5-story steel building using E-defense shake table. In: International conference for behavior of steel structures in seismic area, Pennsylvania, USA; 2009.
[3] Fahnestock LA, Ricles JM, Sause R. Experimental evaluation of a large-scale buckling-restrained braced frame. J Struct Eng, ASCE 2007;133(9):1205–14.

[4] Uang C-M, Kiggins S. Reducing residual drift of buckling-restrained braced frames. In: Int workshop on steel and concrete composite construction, Report No. NCREE-03-026. Taiwan: National Taiwan University; 2003.
[5] Tremblay R, Lacerte M, Christopoulos C. Seismic response of multistory buildings with self-centering energy dissipative steel braces. J Struct Eng, ASCE 2008;134:108–20.
[6] Priestley MJN, Sritharan S. Preliminary results and conclusions from the PRESSS five-story precast concrete test building. PCI J 1999;44(6):42–67.
[7] Ricles JM, Sause R, Garlock MM, Zhao C. Posttensioned seismic-resistant connections for steel frames. J Struct Eng, ASCE 2001;127(2):113–21.
[8] Christopoulos C, Filiatrault A, Uang C-M, Folz B. Posttensioned energy dissipating connections for moment-resisting steel frames. J Struct Eng, ASCE 2002;128(9):1111–20.
[9] Chou C-C, Chen J-H, Chen Y-C, Tsai K-C. Evaluating performance of post-tensioned steel connections with strands and reduced flange plates. Earthquake Eng Struct Dynam 2006;35(9):1167–85.
[10] Chou C-C, Chen Y-C. Tests of post-tensioned precast CFT segmental bridge columns with unbonded strands. Earthquake Eng Struct Dynam 2006;35:159–75.
[11] Chou C-C, Chang H-J, Hewes J. Two-plastic-hinge and two dimensional finite element models for post-tensioned precast concrete segmental bridge columns. Eng Struct 2013;46:205–17.
[12] Chou C-C, Weng C-Y, Chen J-H. Seismic design and behavior of post-tensioned connections including effects of a composite slab. Eng Struct 2008;30:3014–23.
[13] Herning G, Garlock MM, Ricles J, Sause R, Li J. An overview of self-centering steel moment frames. In: Proceedings of the structures congress, Austin, TX; 2009.
[14] Chou C-C, Chen J-H. Seismic design and shake table tests of a steel post-tensioned self-centering moment frame with a slab accommodating frame expansion. Earthquake Eng Struct Dynam 2011;40(11):1241–61.
[15] Chou C-C, Chen Y-C. Development of steel dual-core self-centering braces: quasi-static cyclic tests and finite element analyses. Earthquake Spectra 2015;31(1):247–72.
[16] Chou C-C, Chen Y-C, Pham DH, Truong VM. Steel braced frames with dual-core SCBs and sandwiched BRBs: mechanics, modeling and seismic demands. Eng Struct 2014;72:26–40.
[17] Chou C-C, Chung P-T. Development of cross-anchored dual-core self-centering braces for seismic resistance. J Constr Steel Res 2014;101:19–32.
[18] Christopoulos C, Tremblay R, Kim HJ, Lacerte M. Self-centering energy dissipative bracing system for the seismic resistance of structures: development and validation. J Struct Eng, ASCE 2008;134(1):96–107.
[19] Chou C-C, Wu T-H, Beato Ovalle RA, Chung P-T, Chen Y-H. Seismic design and tests of a full-scale one-story one-bay steel frame with a dual-core self-centering brace. Eng Struct 2016;111:435–50.
[20] Miller DJ, Fahnestock LA, Eatherton MR. Development and experimental validation of a nickel-titanium shape memory self-centering buckling-restrained brace. Eng Struct 2012;40:288–98.
[21] Liu L, Wu B. Self-centering buckling-restrained braces. Adv Mater Res 2013;639–640:846–9.
[22] Zhou Z, He X-T, Wu J, Wang C-L, Meng S-P. Development of a novel self-centering buckling-restrained brace with BFRP composite tendons. Steel Compos Struct Int J 2014;16(5):491–506.
[23] Eatherton MR, Fahnestock LA, Miller DJ. Computational study of self-centering buckling-restrained braced frame seismic performance. Earthquake Eng Struct Dynam 2014;43(13):1897–914.
[24] Chou C-C, Chen S-Y. Subassemblage tests and finite element analyses of sandwiched buckling-restrained braces. Eng Struct 2010;32:2108–21.
[25] Chou C-C, Liu J-H, Pham DH. Steel buckling-restrained braced frames with single and dual corner gusset connections: seismic tests and analyses. Earthquake Eng Struct Dynam 2012;7(41):1137–56.
[26] Chou C-C, Chung P-T, Cheng Y-T. Seismic tests of large-scale energy dissipating braces: dual-core self-centering brace and sandwiched buckling-restrained brace. In: 5th Asia conference on earthquake engineering, October 16–18, Taiwan; 2014.
[27] AISC. Seismic provisions for structural steel buildings. Chicago, IL: American Institute of Steel Construction; 2010.
[28] Priestley MJN, Seible F, Calvi GM. Seismic design and retrofit of bridges. John Wiley & Sons Inc; 1996.
[29] ASCE Standard. Minimum design loads for building and other structures. American Society of Civil Engineers; 2010.
[30] Benavent-Climent A. An energy-based method for seismic retrofit of existing frames using hysteretic dampers. Soil Dynam Earthquake Eng 2011;31:1385–96.
[31] Chou C-C, Uang C-M. A procedure for evaluating seismic energy demand of framed structures. Earthquake Eng Struct Dynam 2003;32:229–44.
[32] Tsai W-J. Development and cyclic tests of cross-anchored dual-core self-centering sandwiched buckling-restrained braces (SC-SBRBs). Thesis Advisor: Chou C-C, Department of Civil Engineering, National Taiwan University, Taiwan; 2014.
[33] Ariyaratana C, Fahnestock AL. Evaluation of buckling-restrained braced frame seismic performance considering reserve strength. Eng Struct 2011;33(1):77–89.
[34] Piedrafita D, Cahis X, Simon E, Comas J. A new modular buckling restrained brace for seismic resistant buildings. Eng Struct 2013;56:1967–75.
[35] Chou C-C, Chung P-T, Cheng Y-T. Experimental evaluation of large-scale dual-core self-centering braces and sandwiched buckling-restrained braces. Eng Struct 2016;116:12–25.

Glossary

ASTM: American Society for Testing and Materials
BRB: buckling-restrained brace
BRBF: buckling-restrained braced frame
CBF: concentrically braced frame
DC-SCB: dual-core self-centering brace
MRF: moment-resistant frame
PT: post-tensioning
SBRB: sandwiched buckling-restrained brace
SC: self-centering
SC-SBRB: self-centering sandwiched buckling-restrained brace
SCED: self-centering energy dissipative